PCCP

Statistical Errors in Reduced Density Matrices Sampled from Quantum Circuit Simulation and the Impact on Multireference Perturbation Theory

Journal:	*Physical Chemistry Chemical Physics*
Manuscript ID	CP-ART-07-2023-003520.R2
Article Type:	Paper
Date Submitted by the Author:	04-Oct-2023
Complete List of Authors:	Nishio, Soichiro; Kyoto University, Oba, Yuki; Kyoto University, Graduate School of Science, Department of Chemistry Kurashige, Yuki; Kyoto University, Graduate School of Science, Department of Chemistry

Statistical Errors in Reduced Density Matrices Sampled from Quantum Circuit Simulation and the Impact on Multireference Perturbation Theory

Soichiro Nishio[1], Yuki Oba[1], and Yuki Kurashige*[1]

[1]Department of Chemistry, Graduate School of Science, Kyoto University, Kitashirakawa Oiwake-cho, Sakyo-ku Kyoto, 606-8502, Japan

October 23, 2023

Abstract

In this work, we present a detailed analysis of statistical errors in reduced density matrices (RDMs) of active space wavefunctions sampled from quantum circuit simulation and the impact on results obtained by the multireference theories. From the sampling experiments, it is shown that the errors in sampled RDMs have larger value for higher-order RDMs, and that the errors in sampled RDMs for excited states are larger than those for the ground state. We analytically derive the expected value of the sum of squared errors between the true distribution and sample distribution of weights of the electron configurations based on a multinomial distribution model, with which we present an assessment of the dependency of RDM errors on the number of shots for the observation (N_{shot}) and on the character of the target electronic state. With the benchmark calculations of short

*Electronic mail: kura@kuchem.kyoto-u.ac.jp

polyenes, C_4H_6 and C_6H_8, we report the statistical errors in CASCI and complete active space second-order perturbation theory (CASPT2) energies obtained with the sampled 1,2-RDMs and 1,2,3,4-RDMs, respectively. It was found that the standard deviation (SD) of the sampled CASCI energies are proportional to $1/\sqrt{N_{\rm shot}}$ as predicted. It was also found that the dependence of the SD of the second-order correction energies are somewhat different but the errors in the reference CASCI energies are dominant as compared with the corrections and the SD of the resulting CASPT2 energies are proportional to $1/\sqrt{N_{\rm shot}}$. It suggests that the required $N_{\rm shot}$ for 3,4-RDMs used only in the second-order perturbative corrections is smaller than that for 1,2-RDM used to calculate the reference CASCI energies. It was also suggested from the analysis of the errors in the sampled energies that the required $N_{\rm shot}$ for 3-RDM, which is used to calculate the perturbative correction energies, can be smaller than that for 2-RDM to calculate the CASCI energies. In fact, it was shown that the potential energy curve along the isomerization reaction of the $\{[Cu(NH_3)_3]_2O_2\}^{2+}$ complex as an archetype of metalloenzyme, in which static and dynamical electron correlation are both important, can be reasonably reproduced with $N_{\rm shot} = 10^6$ for 1,2-RDMs but $N_{\rm shot} = 10^5$ for 3-RDM by the sampling simulation.

1 Introduction

Within the framework of molecular orbital theory, the exact solution of the time-independent Schrödinger equation with a fixed basis set is provided by the Full Configuration Interaction (Full-CI) method. The Full-CI wavefunction is expanded by all possible electron configurations, the number of which increases with the number of combinations between orbitals and electrons. This leads to a complete consideration of electron correlation, however, the computational costs increase exponentially with the size of the system. Application of the Full-CI wavefunction is limited to small systems only. In order to efficiently account for the electron correlation while keeping the computational cost affordable, various wavefunction theories have been developed; [1–3] the Complete active space (CAS) wavefunction is one of the most commonly used wavefunction methods. [4] In the CAS wavefunction, the molecular orbitals are divided into three sets: The inactive orbitals, which are always doubly occupied by electrons; the virtual

orbitals, which are not occupied by electrons; and the active orbitals, which can be either occupied or unoccupied in the CI expansion. By limiting the number of active orbitals and active electrons and performing the Full-CI calculation within this reduced Hilbert space (which is called an active space), an efficient approximation to the Full-CI wavefunction is obtained; this is called the CASCI (CAS Configuration Interaction) method. In the CASCI calculation, the strong electron correlation of nearly degenerate electron configurations within the active space, known as the static electron correlation, can be efficiently described. However, in many cases, it is known that considering only the static electron correlation is insufficient for quantitative prediction of molecular energies. To account for the electron correlation that is neglected in CASCI, i.e., the correlation between the electron configurations inside and outside the active space, a second-order perturbation theory based on the CAS wavefunction, called CASPT2 (CAS second-order perturbation theory), has been developed. [5] This additional correlation is often referred to as the dynamical electron correlation. In many cases, accounting both of statical and dynamical correlation energy is necessary to obtain results with chemical accuracy, that is, 1.0 kcal/mol or 0.05 eV for a single molecule. It should be noted that although the CAS wavefunction is an efficient approximation to Full CI, the dimensionality of the active space still increases exponentially with the combinations of active orbitals and active electrons; the curse of dimensionality is again an obstacle to the application of the CAS wavefunction to large systems. With the advent of the Density Matrix Renormalization Group (DMRG) combined with the CAS wavefunction, [6–9] the computationally feasible size of CAS space has significantly improved. However, the computational cost for the DMRG-CAS wavefunction scales exponentially for two- (or more) dimentional sytems, because efficient trancation of the number of the renormalized many-body basis states is difficult in these cases.

Simulation of the Hamiltonian for strongly entangled quantum systems is widely regarded as a promising application [10–18] in both Noisy Intermediate-Scale Quantum (NISQ) devices [19–24] and Fault-Tolerant Quantum Computers (FTQC), [25–28] which has the potential to enable calculations for large CAS wavefunctions that are difficult to achieve with classical computers. By associating an electronic configuration in the active space with an

eigenstate of qubits, it is possible to map a CAS wavefunction onto a superposition state of qubits; the required number of qubits is equal to the number of spin-orbitals in the active space. For the implementation of quantum circuits, the reduction of Hilbert space by the CAS wavefunction is desirable because the number of required qubits is reduced. [29] As a result, it is expected that calculations of large CAS wavefunctions can be efficiently performed by using a linearly scalable number of qubits.

As will be mentioned in detail in the subsequent section, the electronic energies of target molecules are calculated by sampling of reduced density matrices (RDMs) for the electrons in the active space orbitals from quantum circuits and subsequently parsing the RDMs to classical computers, [30–33] which is often called as a quantum-classical hybrid algorithm. For the CAS wavefunctions represented on qubits, these active-space RDMs are obtained by repeatedly observing the superposition states on the qubits and statistical estimation; if an infinite number of observations is performed, an exact RDM will be obtained. In this RDM sampling, errors are expected to occur due to two main factors; the first is hardware errors, such as thermal fluctuations and the fidelity of quantum gate operations; the second is the statistical error that results from estimating quantum superposition states by a finite number of observations. There are a couple of previous studies on these problems of errors which are closely related to the work of the present paper; in ref. [34], a robust algorithm using the Tensor Product Basis (TPB) representation [35] of Pauli operators, and sampling simulation of 1- and 2-RDMs are proposed; in ref. [36], a demonstration of NEVPT2 [37, 38] calculations using the RDM obtained by simulating the observation of the wavefunction on qubits is conducted, aiming to evaluate the impact of RDM observation errors on the NEVPT2 energy; also in ref. [32] a calculation with the NEVPT2 method is presented, with remarkable demonstration with quantum devices. In this work of ours, we focus on two unresolved aspects among these previous studies; one is the dependency of the statistical errors in sampled RDM on the number of shots in the measurement, as well as on the character of electronic state such as the ground state and the excited states; the other is the evaluation of non-trivial energy errors when sampled RDMs are applied to the subsequent CASPT2 method. The strongly-contracted

(SC-)NEVPT2, which is used in ref. [36], and CASPT2 have different constructions of the internal contracted basis (ICB), and therefore, it is expected that the errors in the reduced density matrix (RDM) will have different impacts on the N-representability and the correction energy. [39–41] In particular, for the dissociation of a nitrogen molecule or for the excited energies of short polyenes, the effect of cumulant approximation for the higher order RDMs cause a significant error in NEVPT2 energy, [36, 39] while the error in the CASPT2 energy is not significant. [42]

These two points should be important aspects when addressing problems in chemistry. It should be mentioned that in most of the previous studies the target systems are the ground state of small molecules consisting of the second-row atoms. Although the results of simple systems provide valuable insights, demonstration on more challenging systems or chemically interesting molecules should be pursued to investigate the possibility of application to more realistic problems in chemistry.

In the present paper, we performed sampling simulation of the active-space RDMs from the CAS wafefunction which is mapped on qubits. We analytically derived the expectation value of the sum of squared errors (SSE) between the sampling results and the corresponding exact solution as a function of the CI coefficients and the number of shots in the measurement, with which we assessed the statistical errors on the sampled RDMs, and analyzed the resulting CASCI energies and CASPT2 energies for the ground state and the excited states of the target molecules. In addition, we discuss the number of shots required to perform CAS calculations on a quantum computer within the range of chemical accuracy. We demonstrated the calculation of the potential energy curve for the isomerisation of the $\{[Cu(NH_3)_3]_2O_2\}^{2+}$ molecule shown in the section 3.3, a challenging molecule with strong entanglement that has rarely been addressed in previous quantum chemistry studies using quantum computers.

2 Method

2.1 Active-space RDMs and CASCI / CASPT2 energies

In the CAS method, the active space Hamiltonian $\hat{\mathcal{H}}_{\mathrm{CAS}}$ is defined as

$$\hat{\mathcal{H}}_{\mathrm{CAS}} = \sum_{pq} h_{pq,\sigma} a^{\dagger}_{p\sigma} a_{q\sigma} + \frac{1}{2} \sum_{pqrs,\sigma\tau} h_{pqrs} a^{\dagger}_{p\sigma} a^{\dagger}_{r\tau} a_{s\tau} a_{q\sigma} + E_0. \tag{1}$$

Here, h_{pq} and h_{pqrs} represent one-electron and two-electron integrals respectively, while $a^{\dagger}_p$ and a_p represent a creation and an annihilation operator for a spatial orbital p. σ and τ represent spin label, and E_0 is a constant energy. The CASCI energy E_{CASCI} for a CAS wavefunction $|\Psi_{\mathrm{CAS}}\rangle$ is written as

$$E_{\mathrm{CASCI}} = \langle \Psi_{\mathrm{CAS}} | \hat{\mathcal{H}}_{\mathrm{CAS}} | \Psi_{\mathrm{CAS}} \rangle \tag{2}$$

$$= \sum_{pq} h_{pq,\sigma} \langle \Psi_{\mathrm{CAS}} | a^{\dagger}_{p\sigma} a_{q\sigma} | \Psi_{\mathrm{CAS}} \rangle + \frac{1}{2} \sum_{pqrs,\sigma\tau} h_{pqrs} \langle \Psi_{\mathrm{CAS}} | a^{\dagger}_{p\sigma} a^{\dagger}_{r\tau} a_{s\tau} a_{q\sigma} | \Psi_{\mathrm{CAS}} \rangle + E_0 \tag{3}$$

$$= \sum_{pq} h_{pq} (\mathbf{\Gamma}^1)_{pq} + \frac{1}{2} \sum_{pqrs} h_{pqrs} (\mathbf{\Gamma}^2)_{pqrs} + E_0. \tag{4}$$

Here, $\mathbf{\Gamma}^1$ and $\mathbf{\Gamma}^2$ are one-particle and two-particle reduced density matrices (1-RDM, 2-RDM) for the active space, respectively. The one-particle reduced density operator and the two-particle reduced density operator are defined as

$$\hat{\Gamma}^1_{pq} \equiv \sum_{\sigma} a^{\dagger}_{p\sigma} a_{q\sigma}, \tag{5}$$

$$\hat{\Gamma}^2_{pqrs} \equiv \sum_{\sigma\tau} a^{\dagger}_{p\sigma} a^{\dagger}_{r\tau} a_{s\tau} a_{q\sigma}. \tag{6}$$

We note that the effect of sampling error in RDMs on the CASCI energy can be estimated by using the formulation below for the sampled RDMs,

$$\mathbf{\Gamma}^n_{\text{sample}} = \mathbf{\Gamma}^n + \delta\mathbf{\Gamma}^n. \tag{7}$$

The error in the resulting CASCI energy δE_{CASCI} is written as

$$\begin{aligned}\delta E_{\text{CASCI}} &= E_{\text{CASCI}}(\mathbf{\Gamma}^1_{\text{sample}}, \mathbf{\Gamma}^2_{\text{sample}}) - E_{\text{CASCI}}(\mathbf{\Gamma}^1, \mathbf{\Gamma}^2) \\ &= \sum_{pq} h_{pq}(\delta\mathbf{\Gamma}^1)_{pq} + \frac{1}{2}\sum_{pqrs} h_{pqrs}(\delta\mathbf{\Gamma}^2)_{pqrs}\end{aligned} \tag{8}$$

The CASPT2 energy is calculated as

$$E_{\text{CASPT2}} = E_{\text{CASCI}} + E_2, \tag{9}$$

where E_2 represents the second-order perturbation energy obtaind by solving the CASPT2 linear equation. [42] For this method, not only 1- and 2-RDMs, but 3-RDMs $\mathbf{\Gamma}^3$ and contracted 4-RDMs $\mathbf{\Gamma}^4$ are required as well.

The number of elements in the n-RDM is equal to $2n$ raised to the power of the number of active orbitals, and the computational cost for 3- and 4-RDMs can be highly expensive for a large CAS space. To perform CASPT2 calculations with an affordable cost one can use cumulant approximation for 3- and 4-RDMs, [42, 43] which is employed in the present work. It should be noted that unlike CASCI energy, CASPT2 energy is not calculated as an expectation value; therefore the effect of statistical errors in RDM on CASPT2 energy is not as obvious as eq.8. In fact, in multireference perturbation theory calculations it is known that errors in higher order RDMs caused by cumulant approximation can break the N-representability condition and cause large errors in the resulting energy. [36, 39, 42]

2.2 Sampling of active-space RDMs from quantum circuit simulation

To perform sampling of active-space RDMs from quantum circuits simulation, the reduced density operators are transformed into a sum of products of Pauli operators by using either the Jordan-Wigner (JW) or Bravyi-Kitaev

(BK) transformation. We note that hereinafter the indices $p, q, ...$ represent the spin-orbitals or the corresponding qubits. The JW transformation is written as

$$a_p^\dagger = P_1^Z \cdots P_{p-1}^Z \frac{1}{2}(P_p^X - jP_p^Y), \tag{10}$$

$$a_p = P_1^Z \cdots P_{p-1}^Z \frac{1}{2}(P_p^X + jP_p^Y), \tag{11}$$

where j is an imaginary unit, P_p^X, P_p^Y, and P_p^Z are Pauli operators acting on the p-th qubit. This allows us to evaluate each element of RDMs using expectation value of the Pauli operators. Furthermore, to make those terms suitable for measurement in the P_p^Z basis, we use the Hadamard matrix H_p and the X-axis rotation matrix on the Bloch sphere at angle θ, $R_p^X(\theta)$, to transform P_p^X and P_p^Y as follows:

$$P_p^X = H_p P_p^Z H_p, \tag{12}$$

$$P_p^Y = R_p^X[-\pi/2] P_p^Z R_p^X[\pi/2]. \tag{13}$$

From eq. (12) and eq. (13), reduced density operators are transformed into linear combinations of products of P_p^Z, H_p, and $R_p^X(\theta)$.

In the following, we show a transformation of a term in one-particle reduced density operator by using eq.(10), (11), (12), and (13) in the case of $a_p^\dagger a_q$ such that $p > q$ for simplicity. By using the commutation relation, the reduced density operator $a_p^\dagger a_q$ is further transformed as follows:

$$
\begin{aligned}
a_p^\dagger a_q = & \frac{1}{4} H_q H_p \left[\prod_{l=q+1}^{p} P_l^Z \right] H_p H_q \\
& + \frac{j}{4} R_q^X[-\pi/2] H_p \left[\prod_{l=q+1}^{p} P_l^Z \right] H_p R_q^X[\pi/2] \\
& - \frac{j}{4} H_q R_p^X[-\pi/2] \left[\prod_{l=q+1}^{p} P_l^Z \right] R_p^X[\pi/2] H_q \\
& + \frac{1}{4} R_q^X[-\pi/2] R_p^X[-\pi/2] \left[\prod_{l=q+1}^{p} P_l^Z \right] R_p^X[\pi/2] R_q^X[\pi/2].
\end{aligned} \tag{14}
$$

See Supporting Information for detailed derivation.

In quantum circuits, an occupation number vector $|\mathbf{k}\rangle = |k_1, \cdots, k_p, \cdots, k_N\rangle$, where k_p is equal to 1 if the p-th spin-orbital is occupied and otherwise 0, is mapped to a direct product of eigenstates of P^Z operators:

$$
|\mathbf{k}\rangle = |k_1, \cdots, k_p, \cdots, k_N\rangle \tag{15}
$$

$$
= |k_1\rangle \otimes \cdots \otimes |k_p\rangle \otimes \cdots \otimes |k_N\rangle . \tag{16}
$$

Here, the number of spin-orbital N is equal to the number of qubits. k_p is equal to 1 if the p-th spin-orbital is occupied; otherwise k_p is equal to 0. $|0\rangle$ and $|1\rangle$ correspond to the eigenstates of P^Z for a qubit, that is,

$$
P^Z |0\rangle = |0\rangle , \tag{17}
$$

$$
P^Z |1\rangle = - |1\rangle . \tag{18}
$$

By associating the CI coefficient $c_{\mathbf{k}}$ with the probability to observe the state $|\mathbf{k}\rangle$, we obtain a representation of the CAS wavefunction in a quantum circuit,

$$
\Psi_{\mathrm{CAS}} = \sum_{\mathbf{k}} c_{\mathbf{k}} |\mathbf{k}\rangle . \tag{19}
$$

By denotating the unitary operators in eq.(14), i.e. H_pH_q, $H_pR_q^X[\pi/2]$, $R_p^X[\pi/2]H_q$, or $R_p^X[\pi/2]R_q^X[\pi/2]$, by U_i, the matrix element for eq.(14) can be transformed as

$$\begin{aligned}
&\langle\Psi_{\mathrm{CAS}}|a_p^\dagger a_q|\Psi_{\mathrm{CAS}}\rangle \\
&= \sum_i A_{U_i} \langle\Psi_{\mathrm{CAS}}|U_i^\dagger \left[\prod_{l=q+1}^{p} P_l^Z\right] U_i|\Psi_{\mathrm{CAS}}\rangle \\
&= \sum_i A_{U_i} \langle\tilde{\Psi}^{U_i}| \left[\prod_{l=q+1}^{p} P_l^Z\right] |\tilde{\Psi}^{U_i}\rangle \\
&= \sum_i A_{U_i} \langle\tilde{\Psi}^{U_i}|(-1)^{\sum_{l=q+1}^{p} k_l}|\tilde{\Psi}^{U_i}\rangle\,, \qquad (20)
\end{aligned}$$

where $|\tilde{\Psi}\rangle$ is a CAS wavefunction transformed by a unitary operator U_i,

$$\begin{aligned}
|\tilde{\Psi}^{U_i}\rangle &= U_i\,|\Psi_{\mathrm{CAS}}\rangle \\
&= U_i \sum_{\mathbf{k}} c_{\mathbf{k}}\,|\mathbf{k}\rangle = \sum_{\mathbf{k}} \tilde{c}_{\mathbf{k}}^{U_i}\,|\mathbf{k}\rangle\,, \qquad (21)
\end{aligned}$$

and A_{U_i} is a coefficient in eq.(14). In the case of eq.(14), A_{U_i} is either of $\frac{1}{4}$, $\frac{j}{4}$, $-\frac{j}{4}$. As a result of the above formula transformation, it is shown that each term of active-space RDMs can be calculated by applying H_p and R_p^X gates to a quantum circuit and measuring it in the P_p^Z basis. We note that each term in eq.(20) can not be simultaneously observed because different U_i yields different $|\tilde{\Psi}^{U_i}\rangle$.

In the sampling simulation of the present work, a CAS wavefunction obtained with classical algorithm is used as the initial state of the quantum circuit simulator, and subsequently transformed into $|\tilde{\Psi}\rangle$ by applying H gates and R^X gates. Subsequently $|\mathbf{k}\rangle$ were sampled from the probability distribution given by $\{|\tilde{c_{\mathbf{k}}^{U_i}}|^2\}$. We note that this sampling of $|\mathbf{k}\rangle$ is equivalent to measurements of CAS wavefunction by the eigenstates of P_p^Z in a real quantum computer with the observation result $|\mathbf{k}\rangle$.

After N_{shot} times of sampling $|\mathbf{k}\rangle$, the CI coefficient for the ON vector $|\mathbf{k}\rangle$ is estimated as

$$|\tilde{c}_{\mathbf{k}}^{U_i}|^2 \approx N_{\mathbf{k}}^i / N_{\text{shot}}, \tag{22}$$

where $N_{\mathbf{k}}^i$ is the number of shots in which $|\mathbf{k}\rangle$ is observed. With eq.(22), and with the occupation of $|\mathbf{k}\rangle$, the resulting matrix element of eq.(20) is estimated,

$$\begin{aligned}
&\langle \Psi_{\text{CAS}} | a_p^\dagger a_q | \Psi_{\text{CAS}} \rangle \\
&= \sum_i A_{U_i} \left(\sum_{\mathbf{k}} (-1)^{\sum_{l=q+1}^{p} k_l} |\tilde{c}_{\mathbf{k}}^{U_i}|^2 \right) \\
&\approx \sum_i A_{U_i} \left(\sum_{\mathbf{k}} (-1)^{\sum_{l=q+1}^{p} k_l} (N_{\mathbf{k}}^i / N_{\text{shot}}) \right).
\end{aligned} \tag{23}$$

We note that higher order RDMs were estimated in the similar way. As the order of the RDM increases, U_i contains more number of H_p and R_p^X; this results in the decrease of the sparsity of $|\tilde{c}_{\mathbf{k}}^{U_i}|^2$. It should be noted that an infinite number of observation gives the exact RDMs for a given CAS wavefunction; with a finite N_{shot}, statistical errors occur in the sampled RDMs obtained. To perform this sampling simulation, we used a in-house code with the PySCF(v2.0.0) package [44], the OpenFermion packege(v1.0.1) [45], and the quantum simulator Qulacs(v0.3.0) [46].

2.3 Statistical errors in the sampled RDMs, CASCI energies, and CASPT2 energies

In order to estimate the statistical errors in the sampled RDMs, we defined the absolute error from the exact n-RDMs as

$$\Delta_{\mathbf{\Gamma}^n} \equiv \frac{\|\mathbf{\Gamma}_{\text{exact}}^n - \mathbf{\Gamma}_{\text{sample}}^n\|_{\text{F}}}{\|\mathbf{\Gamma}_{\text{exact}}^n\|_{\text{F}}} \times 100, \tag{24}$$

where $\mathbf{\Gamma}_{\text{exact}}^n$ is the exact n-RDM, $\mathbf{\Gamma}_{\text{sample}}^n$ is a sampled RDM with N_{shot} fixed, and $\|\|_{\text{F}}$ indicates Frobenius norm. From the sampled 1-, 2-, and 3-RDMs, each of $\Delta_{\mathbf{\Gamma}^n}$, CASCI energy, and CASPT2 energy is calculated for N_{sample}

times, from which we estimate statistical errors by calculating sample mean $\bar{x}$ and standard deviation (SD) σ for each sampled quantitiy. In the present work, the CASPT2 energy with cumulant approximation for 4-RDMs (cu(4)-CASPT2), and that with cumulant approximation for 3- and 4-RDMs (cu(3,4)-CASPT2) are calculated with sampled 1-, 2-, and 3-RDMs and the CASPT2 module of a modified version of the ORZ package. [47]

3 Results

3.1 The distribution of the absolute error in sampled RDMs

For the assessment of errors in the RDMs obtained by quantum circuit sampling simulator of this work, $\Delta_{\mathbf{\Gamma}^n}$ defined in eq.(24), and errors in the corresponding CASCI, cu(4)-CASPT2, and cu(3,4)-CASPT2 energies, we performed benchmark calculations for the ground state and low-lying excited state of all-trans short polyenes, C_4H_6 and C_6H_8 systems. Here the full valence-π active space consists of four electrons in four π-orbitals for C_4H_6, and six electrons in six π-orbitals for C_6H_8; the cc-pVDZ basis set was used. The number of required qubits in the simulations is equal to the number of spin-orbitals in the active space, that is, eight qubits for C_4H_6 and twelve qubits for C_6H_8.

We first investigated the convergence behaviour of sampled CASCI energy for the ground state ($1A_g^-$) of the polyenes with fixed N_{shot} with respect to N_{sample}. The value of N_{sample} that is sufficient for the sample-mean energy to converge within the chemical accuracy (1.0 kcal/mol) to the energies with the exact RDMs is determined to be 100 for $N_{\mathrm{shot}} = 10^3$ and $N_{\mathrm{shot}} = 10^4$, and 20 for $N_{\mathrm{shot}} = 10^5, 10^6$. In the following calculations, N_{sample} are fixed to these values according to the corresponding N_{shot}. See Supporting Information for detail. Note that the mean of the sampled RDMs will coincide with the exact RDM if an infinite number of samples are taken.

For both C_4H_6 and C_6H_8 molecules, $\Delta_{\mathbf{\Gamma}^n}$ for $n = 1, 2, 3$ are calculated for $1A_g^-$, $2A_g^-$ (two electrons excitation from HOMO to LUMO), and $1B_u^+$ (one electron excitation from HOMO to LUMO) states. Fig. 1 shows the sample mean, the SD, and the frequencies of $\Delta_{\mathbf{\Gamma}^n}$ in the form of a violin plot. Comparison between the electronic states

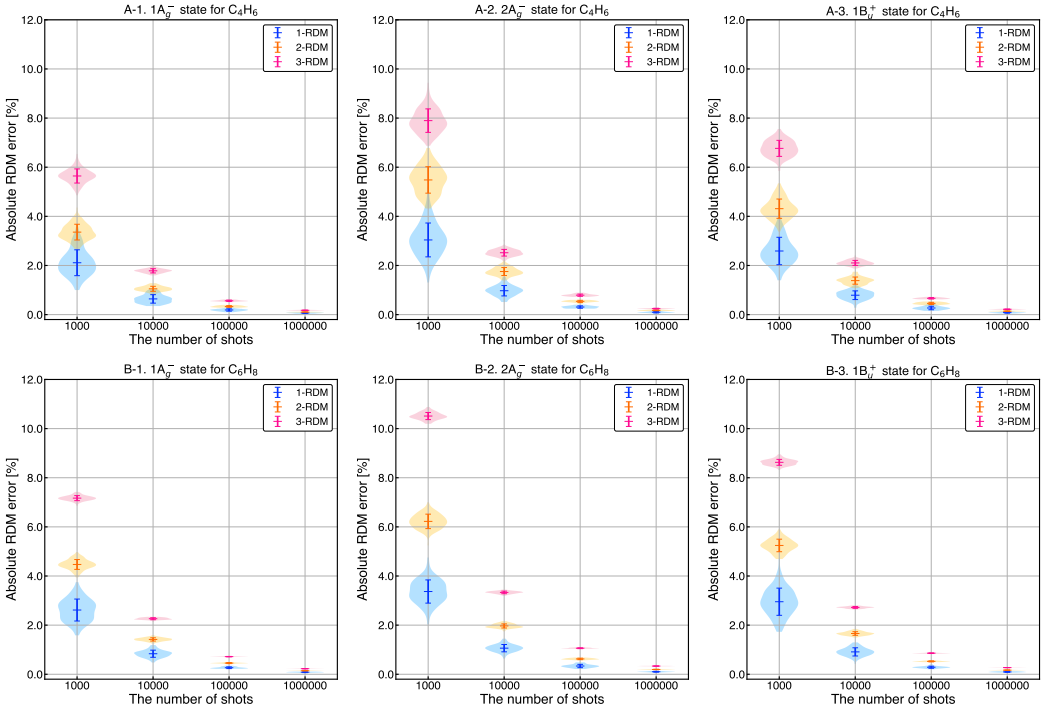

Figure 1: The absolute RDM error $\Delta_{\mathbf{\Gamma}^n}$ for C_4H_6 and C_6H_8. The error bars indicate 1σ in $\Delta_{\mathbf{\Gamma}^n}$.

shows that the $\Delta_{\mathbf{\Gamma}^n}$ for excited states $2A_g^-$ and $1B_u^+$ are larger than those for $1A_g^-$. To investigate the origin of this relationship, we derived the expectation value of the SSE between $|\tilde{c}_{\mathbf{k}}^{U_i}|^2$ and $N_{\mathbf{k}}/N_{\text{shot}}$ in eq.(22). The expectation value of the SSE is given in the form as

$$\mathbb{E}[\text{SSE}] = \frac{1 - \sum_{\mathbf{k}} |\tilde{c}_{\mathbf{k}}^{U_i}|^4}{N_{\text{shot}}}. \tag{25}$$

See Supporting Information for detailed derivation. From this equation, we can evaluate the efficiency at which the observed values $\{N_{\mathbf{k}}^i/N_{\text{shot}}\}$ converge to the target probability distribution $\{|\tilde{c}_{\mathbf{k}}^{U_i}|^2\}$. The convergence is slow if the value of eq.(25) is large, which means that the expectation value of error in sampling of eq.(22) is large; it is also expected from eq.(25) that as the size of the numerator increases, the value of N_{shot} required to obtain sampled RDMs within a given $\Delta_{\mathbf{\Gamma}^n}$ will also increase. It is obvious that $\mathbb{E}[\text{SSE}]$ takes the minimum value 0 when a single component of $\{|\tilde{c}_{\mathbf{k}}^{U_i}|^2\}$ is 1 and the others are 0; $\mathbb{E}[\text{SSE}]$ takes the maximum value $\frac{1-2^{-N}}{N_{\text{shot}}}$ (see eq.(16))

when each component of $\{|\tilde{c}_{\mathbf{k}}^{U_i}|^2\}$ has the same value. From this point it suggests that $\Delta_{\mathbf{\Gamma}^n}$ has greater value for a CAS wavefunction that contains greater number of $|\mathbf{k}\rangle$ with a large weight $|\tilde{c}_{\mathbf{k}}^{U_i}|^2$, i.e., "multi-configurational", because of slow convergence of the observed $\{N_{\mathbf{k}}^i/N_{\rm shot}\}$ vector to the true $\{|\tilde{c}_{\mathbf{k}}^{U_i}|^2\}$. Considering that the number of electron configurations with large weight in the excited state CAS wavefunction is greater than that for the ground state, the electronic state dependence of $\Delta_{\mathbf{\Gamma}^n}$ in Fig.2, i.e., excited states have larger $\Delta_{\mathbf{\Gamma}^n}$ than the ground states, is reasonably explained from eq.(25).

From Fig. 1, it is also seen that the higher order RDMs have larger $\Delta_{\mathbf{\Gamma}^n}$, that is, $\Delta_{\mathbf{\Gamma}^3} > \Delta_{\mathbf{\Gamma}^2} > \Delta_{\mathbf{\Gamma}^1}$. This can be explained with eq.(25) as well. As the number of creation / annihilation operators in the RDM grows, more H and $R_X[-\pi/2]$ gates are applied to $|\Psi_{\rm CAS}\rangle$ with CI coefficients $\{c_{\mathbf{k}}^{U_i}\}$ to obtain $|\tilde{\Psi}^{U_i}\rangle$; by definition, one-qubit gates act to split a single CI coefficient into two configurations; this causes broadening of CI coefficient distribution and results in a greater value of $\mathbb{E}$[SSE] in eq.(25).

The expectation value of squared error for a single $|\mathbf{k}\rangle$ is written as

$$\mathbb{E}\left[\left(|\tilde{c}_{\mathbf{k}}^{U_i}|^2 - \frac{N_{\mathbf{k}}}{N_{\rm shot}}\right)^2\right] = \frac{|\tilde{c}_{\mathbf{k}}^{U_i}|^2 - |\tilde{c}_{\mathbf{k}}^{U_i}|^4}{N_{\rm shot}}. \tag{26}$$

Assuming that the expectation value for $|\tilde{c}_{\mathbf{k}}^{U_i}|^2 - \frac{N_{\mathbf{k}}}{N_{\rm shot}}$ is approximately $(\pm)\sqrt{\frac{|\tilde{c}_{\mathbf{k}}^{U_i}|^2 - |\tilde{c}_{\mathbf{k}}^{U_i}|^4}{N_{\rm shot}}}$, the error in the expectation value of eq.(23) is estimated as

$$\begin{aligned}
&\mathbb{E}\big[\,\langle\Psi_{\rm CAS}|a_p^\dagger a_q|\Psi_{\rm CAS}\rangle - \langle\Psi_{\rm CAS}|a_p^\dagger a_q|\Psi_{\rm CAS}\rangle_{\rm sample}\,\big] \\
&\approx \sum_i a_{U_i}\left(\sum_{\mathbf{k}}(-1)^{\sum_{l=q+1}^p k_l}\sqrt{\frac{|\tilde{c}_{\mathbf{k}}^{U_i}|^2 - |\tilde{c}_{\mathbf{k}}^{U_i}|^4}{N_{\rm shot}}}\right) \\
&= \frac{1}{\sqrt{N_{\rm shot}}}\sum_i a_{U_i}\left(\sum_{\mathbf{k}}(-1)^{\sum_{l=q+1}^p k_l}\sqrt{|\tilde{c}_{\mathbf{k}}^{U_i}|^2 - |\tilde{c}_{\mathbf{k}}^{U_i}|^4}\right),
\end{aligned} \tag{27}$$

thus the $\Delta_{\mathbf{\Gamma}^n}$ dependence on $N_{\rm shot}$ is

$$\Delta_{\Gamma^n} \propto \frac{1}{\sqrt{N_{\rm shot}}}. \tag{28}$$

In the next subsection we show the effect of eq.(28) in the resulting CASCI energies and CASPT2 energies.

3.2 The CASCI energy and the CASPT2 energy dependence on $N_{\rm shot}$

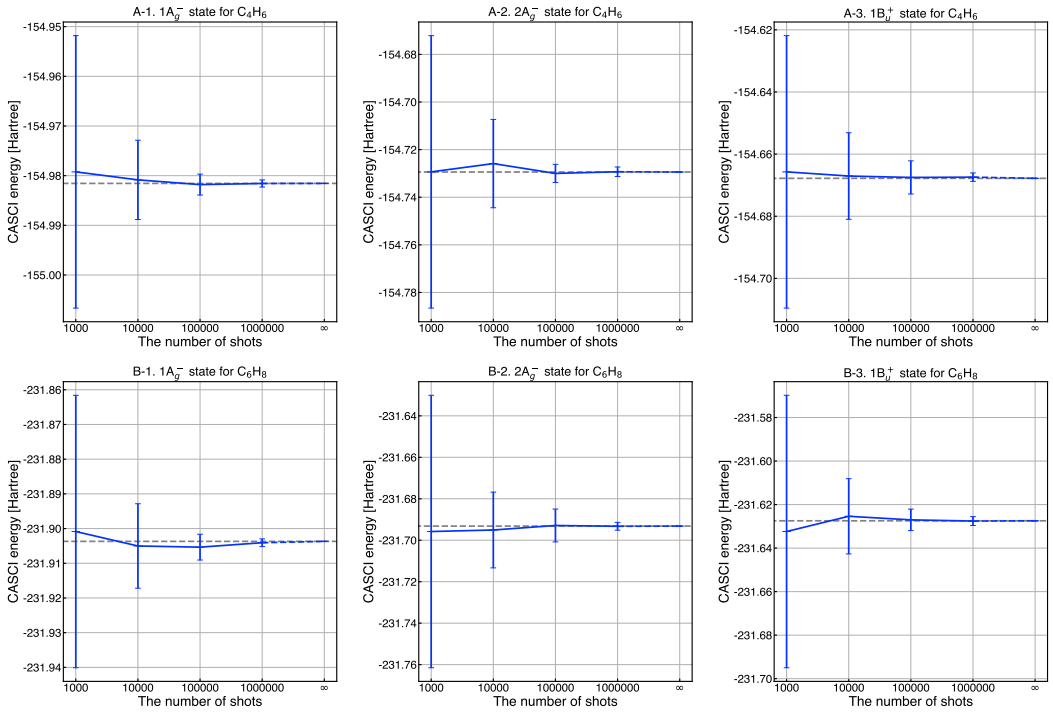

Figure 2: Means and SDs of $E_{\rm CASCI}$ obtained from the sampled RDMs. The exact $E_{\rm CASCI}$ are plotted with dashed lines. The error bars indicate 1σ in the sampled energies.

By using the sampled RDMs, we estimated the errors in the resulting energy from CASCI, cu(4)-CASPT2, and cu(3,4)-CASPT2 methods. Fig. 2 shows the $N_{\rm shot}$ dependence of the CASCI energies for each electronic state of the molecules. The energies obtained from the exact RDMs are plotted with dashed lines. It is shown that the SD of the sampled CASCI energies decreases as $N_{\rm shot}$ increase. By performing least squares fitting on the SD of CASCI energies it was found that this SD is proportional to $1/\sqrt{N_{\rm shot}}$ with $R^2 > 0.997$, which is consitent with

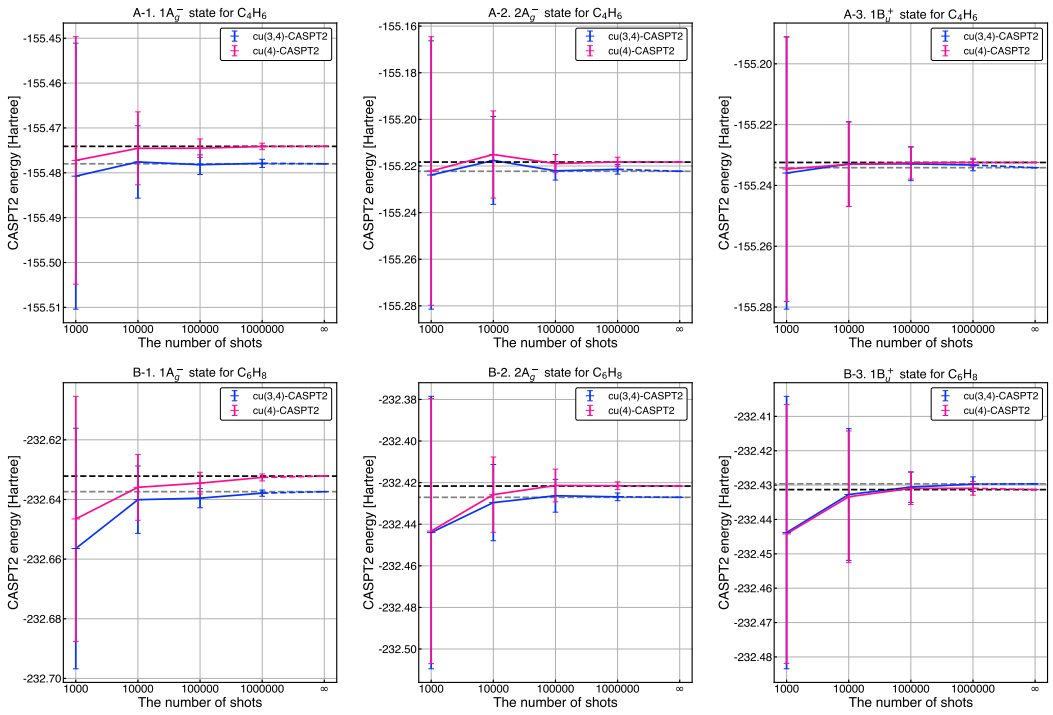

Figure 3: Means and SDs of cu(4)- and cu(3,4)-CASPT2 energies obtained from the sampled RDMs. The exact energies are plotted with dashed lines. The error bars indicate 1σ in the sampled energies.

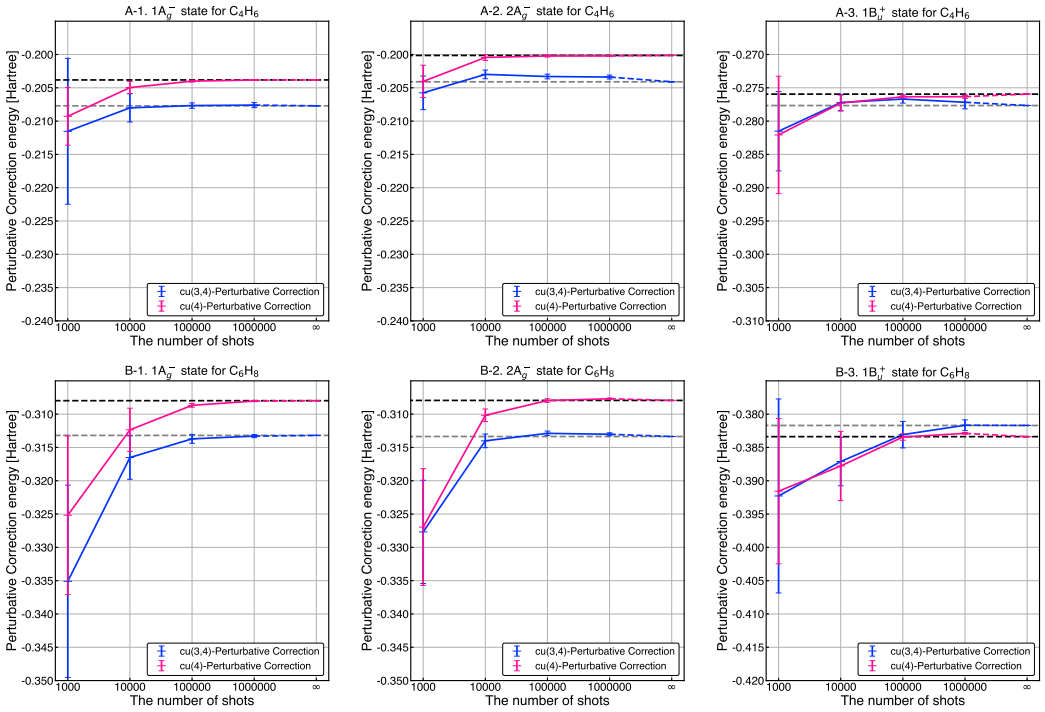

Figure 4: Means and SDs of perturbative correction E_2 obtained with the sampled RDMs. The exact E_2 are plotted with dashed lines. The error bars indicate 1σ in the sampled energies. The contribution from (c, c, v, v) subspace, which is constant with respect to the sampled RDMs, is omitted.

the prediction in eq.(8) eq.(27); we can see that $1/\sqrt{N_{\rm shot}}$ in the error on a single element in $\mathbf{\Gamma}^n$ can be factored out of the summation over the spin-orbital indices in eq.(8).

Fig. 3 shows the $N_{\rm shot}$ dependence of the cu(4)-CASPT2 (megenta) and cu(3,4)-CASPT2(blue) energies. The energies obtained with the exact RDMs are plotted with dashed lines as well. We note that these energies are obtained with (non-variational) single-state CASPT2-D (SS-CASPT2-D) method with the imaginary shift at 0.10 i a.u. and the IPEA shift at 0.25 a.u. applied. It should also be mentioned that the non-variational energies are plotted in order to reduce the instability caused by the level shift and to focus the discussion on the issue of statistical errors.

From Fig. 3, it can be seen that the variation in size of the SDs in both of cu(4)- and cu(3,4)-CASPT2 energies are similar to those of CASCI energies; from Fig. 4, however, it can be seen that the variation in size of the SDs of E_2 is not similar to that of the sampled CASCI energies. This suggests that the errors in the perturbative correction energy is small enough compared to the errors in the CASCI energy and the total CASPT2 energy,

$$\sigma(E_{\rm CASCI}) > \sigma(E_2), \tag{29}$$

$$E_{\rm CASPT2} \gg \sigma(E_2). \tag{30}$$

Here we used a notation $\sigma(X)$ here to represent the SD of quantitiy X. From eq.(29) and eq.(30), it is predicted that the required $N_{\rm shot}$ to achieve chemical accuracy can be smaller for $\sigma(E_2)$ than that of $E_{\rm CASPT2}$; in other words, the effect of the errors in E_2 on $E_{\rm CASPT2}$ is relatively small. By performing least squares fitting, we found that the SDs for sampled cu(4)- and cu(3,4)-CASPT2 energies is propotional to $1/\sqrt{N_{\rm shot}}$, with the minimum $R^2 = 0.9593$ for the case of cu(4)-CASPT2 for the $1B_u^+$ state of C_6H_8. In Table 1, estimated $N_{\rm shot}$ to achieve the SD less than 0.1 eV for the CASCI, cu(4)-CASPT2, cu(3,4)-CASPT2, cu(4)-E_2, and cu(3,4)-E_2 energies are tabulated. In almost all cases, the required numbers of $N_{\rm shot}$ for cu(4)-E_2 and cu(3,4)-E_2 to converge within 0.1 eV to the exact value

are less than those for cu(4)-CASPT2, cu(3,4)-CASPT2, and cu(4)-E_2 energies, which supports the prediction from eq.(29) and eq.(30).

Table 1: Estimated N_{shots} to achieve the SD less than 0.1 eV for the CASCI, cu(4)-CASPT2, cu(3,4)-CASPT2, cu(4)-E_2, and cu(3,4)-E_2 energies. The values for the CASCI, cu(4)-CASPT2, and cu(3,4)-CASPT2 are obtained from the least squares fitting. The values for cu(4)-E_2 and cu(3,4)-E_2 are estimated from the magnitude of the SDs. Note that cu(4)-E_{CASPT2} = E_{CASCI}+cu(4)-E_2.

		E_{CASCI}	cu(4)-E_{CASPT2}	cu(3,4)-E_{CASPT2}	cu(4)-E_2	cu(3,4)-E_2
	$1A_g^-$	5.74×10^4	5.81×10^4	6.71×10^4	$< 10^4$	$< 10^4$
C_4H_6	$2A_g^-$	2.48×10^5	2.52×10^5	2.50×10^5	$< 10^3$	$< 10^3$
	$1B_u^+$	1.40×10^5	1.38×10^5	1.44×10^5	$< 10^4$	$< 10^4$
	$1A_g^-$	1.15×10^5	1.28×10^5	1.24×10^5	$< 10^4$	$< 10^4$
C_6H_8	$2A_g^-$	3.17×10^5	2.97×10^5	3.15×10^5	$< 10^4$	$< 10^4$
	$1B_u^+$	2.97×10^5	9.56×10^4	1.09×10^5	$< 10^5$	$< 10^4$

3.3 Estimation of the potential energy curves along the reaction coordinate for the isomarization of $\{[Cu(NH_3)_3]_2O_2\}^{2+}$ molecule

In order to investigate the effect of dynamical correlation on the chemical energy obtained with the quantum circuit sampling simulation of this work, we plotted the ground state energy for $\{[Cu(NH_3)_3]_2O_2\}^{2+}$ complex along the reaction coordinate of the isomerization as shown in Fig. 5. Because of the strongly correlated electrons in this complex, an accurate estimation of the (monomeric) energy difference between A: bis(μ-oxo) and B: μ-η^2:η^2-peroxo form has been a challenging problem for electronic structure methods. [42, 48–52]

In our calculations, the CAS space is constructed from eight electrons in six orbitals, including two $2p_x$ orbitals of

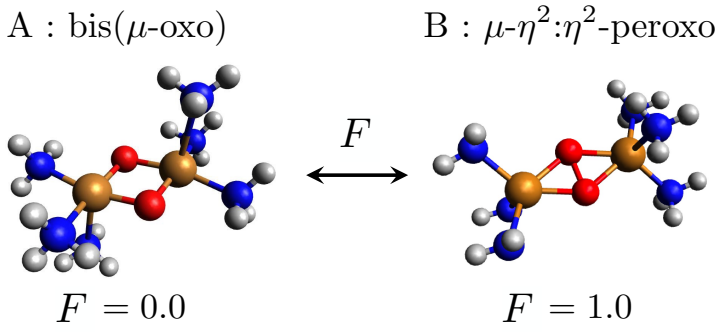

Figure 5: The isomarization scheme of $\{[Cu(NH_3)_3]_2O_2\}^{2+}$ molecule. A: bis(μ-oxo) form is a dimeric Cu complex bridged by two O atoms, where Cu-Cu distance is 2.80 Åand O-O distance is 2.30 Å. B: μ-η^2:η^2-peroxo form is a dimeric Cu complex bridged by a peroxo legand that forms η^2 bonds with each Cu atoms, where Cu-Cu distance is 3.71 Åand O-O distance is 1.46 Å. The coordinate F is defined by interpolating between A form and B form.

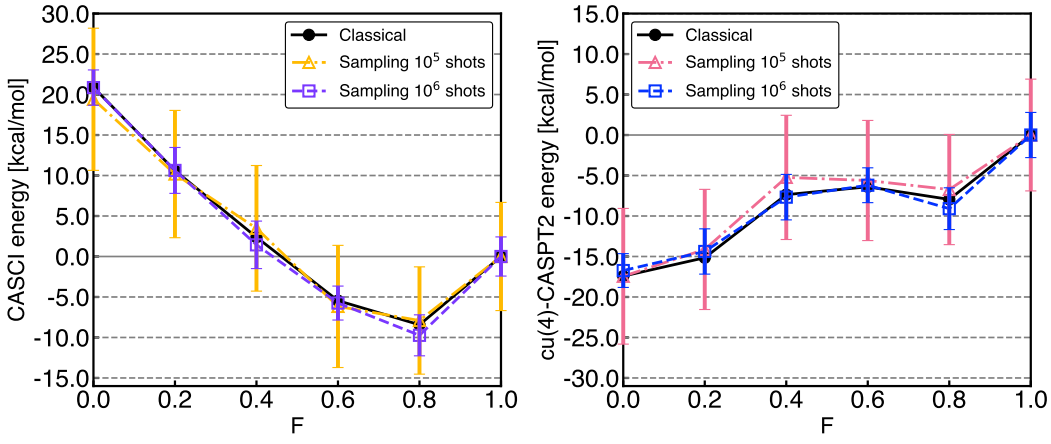

Figure 6: The potential energy curves along the reaction coordinate F for the isomarization of $\{[Cu(NH_3)_3]_2O_2\}^{2+}$ molecule. The error bars indicate 1σ in the sampled energies.

O atoms, two $2p_y$ orbitals of O atoms, and two $3d_{xy}$ orbitals of Cu atoms; N_{shot} is fixed to 10^5 and 10^6, and N_{sample} is fixed to 20; with the cc-pVDZ basis sets, we performed the sampling of 1-, 2-, and 3-RDMs and the corresponding CASCI energy and cu(4)-CASPT2 energy. The CASPT2 energies are obtained with (non-variational) single-state CASPT2-D (SS-CASPT2-D) method with the imaginary shift at 0.10 i a.u. and the IPEA shift at 0.25 a.u. applied. This procedure is performed for the six structures along the reaction coordinates with $F = 0.0$ (the isomer A in Fig.5), 0.2, 0.4, 0.6, 0.8, and 1.0(the isomer B in Fig.5), which are defined in ref. [51].

Fig. 6 shows the potential energy curves (PECs) from CASCI energy and cu(4)-CASPT2 energy. Compared to the CASCI and CASPT2 calculations with CAS(16e,14o) in ref. [42], it is shown that both of our CASCI and CASPT2 results reproduce qualitatively the relative energy between the isomer A and the isomer B even with the small active space. However, it should be noted that the PEC from DMRG-CASPT2 calculation with CAS(24e,28o) in ref. [42], which is the most reliable data with the largest CAS space, is significantly different from the CASPT2 calculations with CAS(16e,14o) and our results. This suggests that a larger CAS space, i.e. more number of qubits in quantum circuit, is necessary to predict qualitatively the PEC of this reaction.

The SD of energies with sampled-RDM is shown in Fig.6 as error bars. Averaged SD of the sampled CASCI energies at each F is 7.54 kcal/mol for $N_{\mathrm{shot}} = 10^5$ and 2.50 kcal/mol for $N_{\mathrm{shot}} = 10^6$; that of the sampled cu(4)-CASPT2 energies is 7.43 kcal/mol for $N_{\mathrm{shot}} = 10^5$ and 2.53 kcal/mol for $N_{\mathrm{shot}} = 10^6$. Considering that the errors in CASPT2 energies are proportional to $1/\sqrt{N_{\mathrm{shot}}}$ as discussed in section 3.2, the minimum N_{shot} required to achieve the chemical accuracy (1.0 kcal/mol $\simeq$ 0.05 eV for a single molecule) in cu(4)-CASPT2 energy averaged for each F is estimated to be 9.6×10^6 shots. We note that the averaged SD of the sampled cu(4)-E_2 at each F is 1.22 kcal/mol for $N_{\mathrm{shot}} = 10^5$ and 0.37 kcal/mol for $N_{\mathrm{shot}} = 10^6$, which suggests that the required N_{shot} for 3-RDM with the chemical accuracy can be smaller one order of magnitude than that of 2-RDM though $\Delta_{\mathbf{\Gamma}^3}$ is larger than $\Delta_{\mathbf{\Gamma}^2}$ as mentioned in Section 3.1.

The required N_{shot} for E_{CASPT2} is larger than that for the calculations of C_6H_8, 1.6×10^6, due to the difference

in the strength of the entanglements in the system molecules. It is interesting that although the required N_{shot} for the chemical accuracy is greater for the Cu complex, the length of the CI vector for the calculation for C_6H_8 (the length is 400) is greater than that for the Cu complex (225). This suggests that depending on the choice of a target system, the contribution of the CAS size to the required N_{shot} for the chemical accuracy can be smaller than that of the distribution of the CI coefficients. A clear explanation is given by comparing the value of numerator in $\mathbb{E}[\mathrm{SSE}]$ in eq.(25); it can be expected that as this value increases, the expected error between $\{|\tilde{c}_{\mathbf{k}}^{U_i}|^2\}$ and $\{N_{\mathbf{k}}^i/N_{\mathrm{shot}}\}$ will also increase, and the required value of N_{shot} for convergence will become larger. The value of numerator is 0.694 for the ground state of the Cu complex at $F = 0.0$ while 0.281 for the ground state of the C_6H_8, which reproduces the relative sizes of the N_{shot} for the chemical accuracy.

It should be mentioned that the PECs may show bumps if the data from the worst sample energy within 1σ at each coordinate are selected; however, by averaging the samples, the mean energies converge to the classical energies, resulting in smooth PECs. Large errors from the break of N-representability condition or from the errors in sampled RMDs are not observed in this simulation.

4 Conclusions

In the present study, we implemented a quantum circuit simulator to observe the RDMs from a CAS wavefunction mapped on qubits. From the sampling experiment, it was shown that the errors in sampled RDMs have larger value for higher-order RDMs, and that errors in RDMs for excited states are larger than those for the ground states. We analytically derived the expectation value of the sum of squared errors between the observation results $\{N^i_{\mathbf{k}}/N_{\mathrm{shot}}\}$ and the exact CI weights distribution $\{|\tilde{c}^{U_i}_{\mathbf{k}}|^2\}$ using a multinomial distribution model, that is, eq.(25), with which we assessed the dependency of RDM errors on N_{shot} and on the character of the target electronic state. As a result of this novel investigation, it was revealed that the larger errors in the excited states and in higher-order RDMs are both explained by the increase in the numerator of eq.(25), $1-\sum_{\mathbf{k}}|\tilde{c}^{U_i}_{\mathbf{k}}|^4$; as the multireference character of the CAS wavefunction increases, the sparsity of the quantum state for the observation decreases, resulting in a larger expectation value of the squared sum of errors; even when the CAS wavefunction has less multireference character, by applying a number of H and R^X operators to obtain the quantum state for the observation with the P^Z eigenstates, the sparsity also decreases.

With the benchmark calculations of C_4H_6 and C_6H_8, we reported that the statistical errors in CASCI energies are proportional to $1/\sqrt{N_{\mathrm{shot}}}$, which is consitent with the prediction from eq.(25) and eq.(26). The convergence of the SD of sampled CASCI and CASPT2 energies and the required N_{shot} to achieve the chemical accuracy are also discussed; in cases where the numerator of eq.(25) has a larger value, i.e. in cases where the target electronic state has more multireference character, a larger N_{shot} is required; from the results shown in Table 1, it is suggested that the required N_{shot} for 3-RDM, which is used to calculate the perturbative correction energies, can be smaller than that for 2-RDM to calculate the E_{CASCI}, though $\Delta_{\mathbf{\Gamma}^3}$ is larger than $\Delta_{\mathbf{\Gamma}^2}$ as mentioned in Section 3.1. It should be emphasized that, to the best of our knowledge, the present study is the first to evaluate the statistical error in the sampled energy for chemically important transition metal complex molecule, where both static and dynamical

electon correlation are important. By demonstrating that the exact PEC of the isomerization of $\{[Cu(NH_3)_3]_2O_2\}^{2+}$ with the same CAS space is reasonably reproduced by the sampling simulation with $N_{\mathrm{shot}} = 10^6$, and by estimating the required N_{shot} to reduce the SD of the sampled CASPT2 energy lower than 3 kcal/mol for 1,2-RDM to be 10^6 and for 3-RDM to be 10^5, our research has made a significant contribution to the future application of similar methods. The CASPT2 energies with sampled RDMs in our simulations did not show significant errors that derive from the break of the N-representability.

Conflict of Interests

The authors declare no conflict of interests.

Data Availability

The data that support the findings of this study are available from the corresponding author upon reasonable request.

Author Contributions

S.N. played a central role in the analysis and interpretation of the data, and also took the lead in the preparation of the manuscript. Y.O. and Y.K. primarily handled the implementation of the simulation code, and Y.O. executed the calculations. Y.K. designed and supervised the work.

Acknowledgements

This work is partly supported by grant-in-aid for Scientific Research (B) (JSPS KAKENHI Grant Number JP19H02675), PRESTO (JST) Grant Number JPMJPR1913, and MEXT Q-LEAP Grant No. JPMXS0120319794.

References

[1] Evangelista FA. Perspective: Multireference Coupled Cluster Theories of Dynamical Electron Correlation. The Journal of Chemical Physics. 2018 Jul;149(3):030901.

[2] Bartlett RJ, Musiał M. Coupled-Cluster Theory in Quantum Chemistry. Reviews of Modern Physics. 2007 Feb;79(1):291-352.

[3] Olsen J. The CASSCF Method: A Perspective and Commentary: CASSCF Method. International Journal of Quantum Chemistry. 2011 Nov;111(13):3267-72.

[4] Roos BO, Taylor PR, Sigbahn PEM. A Complete Active Space SCF Method (CASSCF) Using a Density Matrix Formulated Super-CI Approach. Chemical Physics. 1980 May;48(2):157-73.

[5] Andersson K, Malmqvist PÅ, Roos BO. Second-order Perturbation Theory with a Complete Active Space Self-consistent Field Reference Function. The Journal of Chemical Physics. 1992 Jan;96(2):1218-26.

[6] White SR. Density Matrix Formulation for Quantum Renormalization Groups. Physical Review Letters. 1992 Nov;69(19):2863-6.

[7] White SR, Martin RL. Ab Initio Quantum Chemistry Using the Density Matrix Renormalization Group. The Journal of Chemical Physics. 1999 Mar;110(9):4127-30.

[8] Chan GKL, Head-Gordon M. Highly Correlated Calculations with a Polynomial Cost Algorithm: A Study of the Density Matrix Renormalization Group. The Journal of Chemical Physics. 2002 Mar;116(11):4462-76.

[9] Kurashige Y, Yanai T. Second-Order Perturbation Theory with a Density Matrix Renormalization Group Self-Consistent Field Reference Function: Theory and Application to the Study of Chromium Dimer. The Journal of Chemical Physics. 2011 Sep;135(9):094104.

[10] Mitarai K, Nakagawa YO, Mizukami W. Theory of Analytical Energy Derivatives for the Variational Quantum Eigensolver. Physical Review Research. 2020 Feb;2(1):013129.

[11] Mizukami W, Mitarai K, Nakagawa YO, Yamamoto T, Yan T, Ohnishi Yy. Orbital Optimized Unitary Coupled Cluster Theory for Quantum Computer. Physical Review Research. 2020 Sep;2(3):033421.

[12] Gao Q, Jones GO, Motta M, Sugawara M, Watanabe HC, Kobayashi T, et al. Applications of Quantum Computing for Investigations of Electronic Transitions in Phenylsulfonyl-Carbazole TADF Emitters. npj Computational Materials. 2021 May;7(1):70.

[13] Chen H, Nusspickel M, Tilly J, Booth GH. Variational Quantum Eigensolver for Dynamic Correlation Functions. Physical Review A. 2021 Sep;104(3):032405.

[14] Rice JE, Gujarati TP, Motta M, Takeshita TY, Lee E, Latone JA, et al. Quantum Computation of Dominant Products in Lithium–Sulfur Batteries. The Journal of Chemical Physics. 2021 Apr;154(13):134115.

[15] Hirai H, Horiba T, Shirai S, Kanno K, Omiya K, Nakagawa YO, et al. Molecular Structure Optimization Based on Electrons–Nuclei Quantum Dynamics Computation. ACS Omega. 2022 Jun;7(23):19784-93.

[16] Fujii K, Mizuta K, Ueda H, Mitarai K, Mizukami W, Nakagawa YO. Deep Variational Quantum Eigensolver: A Divide-And-Conquer Method for Solving a Larger Problem with Smaller Size Quantum Computers. PRX Quantum. 2022 Mar;3(1):010346.

[17] Omiya K, Nakagawa YO, Koh S, Mizukami W, Gao Q, Kobayashi T. Analytical Energy Gradient for State-Averaged Orbital-Optimized Variational Quantum Eigensolvers and Its Application to a Photochemical Reaction. Journal of Chemical Theory and Computation. 2022 Feb;18(2):741-8.

[18] D'Cunha R, Crawford TD, Motta M, Rice JE. Challenges in the Use of Quantum Computing Hardware-Efficient Ansätze in Electronic Structure Theory. The Journal of Physical Chemistry A. 2023 Apr;127(15):3437-48.

[19] Preskill J. Quantum Computing in the NISQ Era and Beyond. Quantum. 2018 Aug;2:79.

[20] Peruzzo A, McClean J, Shadbolt P, Yung MH, Zhou XQ, Love PJ, et al. A Variational Eigenvalue Solver on a Photonic Quantum Processor. Nature Communications. 2014 Sep;5(1):4213.

[21] Bauer B, Wecker D, Millis AJ, Hastings MB, Troyer M. Hybrid Quantum-Classical Approach to Correlated Materials. Physical Review X. 2016 Sep;6(3):031045.

[22] Kandala A, Mezzacapo A, Temme K, Takita M, Brink M, Chow JM, et al. Hardware-Efficient Variational Quantum Eigensolver for Small Molecules and Quantum Magnets. Nature. 2017 Sep;549(7671):242-6.

[23] Babbush R, Wiebe N, McClean J, McClain J, Neven H, Chan GKL. Low-Depth Quantum Simulation of Materials. Physical Review X. 2018 Mar;8(1):011044.

[24] Nakanishi KM, Mitarai K, Fujii K. Subspace-Search Variational Quantum Eigensolver for Excited States. Physical Review Research. 2019 Oct;1(3):033062.

[25] Lloyd S. Universal Quantum Simulators. Science. 1996 Aug;273(5278):1073-8.

[26] Aspuru-Guzik A, Dutoi AD, Love PJ, Head-Gordon M. Simulated Quantum Computation of Molecular Energies. Science. 2005 Sep;309(5741):1704-7.

[27] Otten M, Hermes MR, Pandharkar R, Alexeev Y, Gray SK, Gagliardi L. Localized Quantum Chemistry on Quantum Computers. arXiv; 2022.

[28] Goings JJ, White A, Lee J, Tautermann CS, Degroote M, Gidney C, et al. Reliably Assessing the Electronic Structure of Cytochrome P450 on Today's Classical Computers and Tomorrow's Quantum Computers. Proceedings of the National Academy of Sciences. 2022 Sep;119(38):e2203533119.

[29] Takeshita T, Rubin NC, Jiang Z, Lee E, Babbush R, McClean JR. Increasing the Representation Accuracy of Quantum Simulations of Chemistry without Extra Quantum Resources. Physical Review X. 2020 Jan;10(1):011004.

[30] Tilly J, Sriluckshmy PV, Patel A, Fontana E, Rungger I, Grant E, et al. Reduced Density Matrix Sampling: Self-consistent Embedding and Multiscale Electronic Structure on Current Generation Quantum Computers. Physical Review Research. 2021 Sep;3(3):033230.

[31] Tilly J, Chen H, Cao S, Picozzi D, Setia K, Li Y, et al. The Variational Quantum Eigensolver: A Review of Methods and Best Practices. Physics Reports. 2022 Nov;986:1-128.

[32] Tammaro A, Galli DE, Rice JE, Motta M. $\underline{N}$ -Electron Valence Perturbation Theory with Reference Wave Functions from Quantum Computing: Application to the Relative Stability of Hydroxide Anion and Hydroxyl Radical. The Journal of Physical Chemistry A. 2023 Jan;127(3):817-27.

[33] Motta M, Jones GO, Rice JE, Gujarati TP, Sakuma R, Liepuoniute I, et al. Quantum Chemistry Simulation of Ground- and Excited-State Properties of the Sulfonium Cation on a Superconducting Quantum Processor. Chemical Science. 2023;14(11):2915-27.

[34] Tilly J, Sriluckshmy PV, Patel A, Fontana E, Rungger I, Grant E, et al. Reduced Density Matrix Sampling: Self-consistent Embedding and Multiscale Electronic Structure on Current Generation Quantum Computers. Physical Review Research. 2021 Sep;3(3):033230.

[35] Hamamura I, Imamichi T. Efficient Evaluation of Quantum Observables Using Entangled Measurements. npj Quantum Information. 2020 Jun;6(1):56.

[36] Krompiec M, Ramo DM. Strongly Contracted N-Electron Valence State Perturbation Theory Using Reduced Density Matrices from a Quantum Computer. arXiv; 2022.

[37] Angeli C, Cimiraglia R, Evangelisti S, Leininger T, Malrieu JP. Introduction of n -Electron Valence States for Multireference Perturbation Theory. The Journal of Chemical Physics. 2001 Jun;114(23):10252-64.

[38] Angeli C, Cimiraglia R, Malrieu JP. N -Electron Valence State Perturbation Theory: A Spinless Formulation and an Efficient Implementation of the Strongly Contracted and of the Partially Contracted Variants. The Journal of Chemical Physics. 2002 Nov;117(20):9138-53.

[39] Zgid D, Ghosh D, Neuscamman E, Chan GKL. A Study of Cumulant Approximations to N-Electron Valence Multireference Perturbation Theory. The Journal of Chemical Physics. 2009 May;130(19):194107.

[40] Harris FE. Cumulant-Based Approximations to Reduced Density Matrices. International Journal of Quantum Chemistry. 2002;90(1):105-13.

[41] Herbert JM. Magnitude and Significance of the Higher-Order Reduced Density Matrix Cumulants. International Journal of Quantum Chemistry. 2007;107(3):703-11.

[42] Kurashige Y, Chalupský J, Lan TN, Yanai T. Complete Active Space Second-Order Perturbation Theory with Cumulant Approximation for Extended Active-Space Wavefunction from Density Matrix Renormalization Group. The Journal of Chemical Physics. 2014 Nov;141(17):174111.

[43] Saitow M, Kurashige Y, Yanai T. Multireference Configuration Interaction Theory Using Cumulant Reconstruction with Internal Contraction of Density Matrix Renormalization Group Wave Function. The Journal of Chemical Physics. 2013 Jul;139(4):044118.

[44] Sun Q, Zhang X, Banerjee S, Bao P, Barbry M, Blunt NS, et al. Recent Developments in the PySCF Program Package. The Journal of Chemical Physics. 2020 Jul;153(2):024109.

[45] McClean JR, Rubin NC, Sung KJ, Kivlichan ID, Bonet-Monroig X, Cao Y, et al. OpenFermion: The Electronic Structure Package for Quantum Computers. Quantum Science and Technology. 2020 Jun;5(3):034014.

[46] Suzuki Y, Kawase Y, Masumura Y, Hiraga Y, Nakadai M, Chen J, et al. Qulacs: A Fast and Versatile Quantum Circuit Simulator for Research Purpose. Quantum. 2021 Oct;5:559.

[47] Yanai T, Kurashige Y, Mizukami W, Chalupský J, Lan TN, Saitow M. Density Matrix Renormalization Group for Ab Initio Calculations and Associated Dynamic Correlation Methods: A Review of Theory and Applications. International Journal of Quantum Chemistry. 2015;115(5):283-99.

[48] Malmqvist PÅ, Pierloot K, Shahi ARM, Cramer CJ, Gagliardi L. The Restricted Active Space Followed by Second-Order Perturbation Theory Method: Theory and Application to the Study of CuO2 and Cu2O2 Systems. The Journal of Chemical Physics. 2008 May;128(20):204109.

[49] Shamasundar KR, Knizia G, Werner HJ. A New Internally Contracted Multi-Reference Configuration Interaction Method. The Journal of Chemical Physics. 2011 Aug;135(5):054101.

[50] Rode MF, Werner HJ. Ab Initio Study of the O2 Binding in Dicopper Complexes. Theoretical Chemistry Accounts. 2005 Oct;114(4-5):309-17.

[51] Cramer CJ, Włoch M, Piecuch P, Puzzarini C, Gagliardi L. Theoretical Models on the Cu $_2$ O $_2$ Torture Track: Mechanistic Implications for Oxytyrosinase and Small-Molecule Analogues. The Journal of Physical Chemistry A. 2006 Feb;110(5):1991-2004.

[52] Flock M, Pierloot K. Theoretical Study of the Interconversion of O $_2$ -Binding Dicopper Complexes. The Journal of Physical Chemistry A. 1999 Jan;103(1):95-102.